2nd International Conference on Engineering Optimization
September 6-9, 2010, Lisbon, Portugal

Durability-based Structural Optimization with Reduced Elastic Multibody Systems

Christoph Tobias, Jörg Fehr and Peter Eberhard

Institute of Engineering and Computational Mechanics
University of Stuttgart
Pfaffenwaldring 9, 70569 Stuttgart, Germany
[christoph.tobias, fehr, eberhard]@itm.uni-stuttgart.de

Abstract
This contribution presents a structural optimization loop comprising reduced elastic multibody system simulation, finite element models and durability analysis. Whereas conventional approaches in this field require a postprocessing of elastic multibody system results, the presented work allows the calculation of damage values during runtime of the elastic multibody system simulation. Here, those quantities are directly computed during the elastic multibody system simulation in order to speed up computation times. An error-free recovery of dynamic stresses for predefined frequencies is assured by a finite element model order reduction based on so-called Krylov-subspaces. This feature represents an innovation compared to conventional structural optimization loops including reduced elastic multibody system simulation. Those modal approaches, which are state of the art, have to struggle with uncertainties of the elastic multibody system results. The developed optimization loop is illustrated with the help of an example.

Keywords: structural optimization, elastic multibody systems, durability analysis, Krylov-subspaces.

1. Introduction

Structural optimization is a capable tool in the design process of mechanical systems. If a structural optimization task is expanded to a dynamic problem, the use of an elastic multibody system (EMBS) is often suitable. In this context, the structure that is to be optimized is often considered as an elastic body which originates from a reduced finite element (FE) model of the structure. In order to obtain a scalar performance criterion for the optimization algorithm, the EMBS results are usually further postprocessed and together with information from the FE model, a durability analysis is carried out. This approach is proposed in (1) and applied e.g. in (2). In this periphery, the following article will describe a shape optimization loop, which is meant to be a further development regarding these works. Special attention is paid to the correct determination of dynamic stresses in the structure that is to be optimized, since durability results are extremely sensitive with respect to them. Furthermore, the optimization loop is simplified by the integration of an 'online' durability analysis in the EMBS. Therewith, the EMBS can directly be interfaced with the optimization algorithm.

2. Overview of the Optimization Process

The optimization loop presented in this contribution and its according workflow is summarized in Figure 1. The structural optimization method, which is used here, is 'parameter free' and based on the FE mesh of the investigated structure, see e.g. (3) or (4). That means, design variables are the positions of the nodes of the FE model which are moved by the optimization algorithm. In many applications the effects of these geometric changes (like an associated variation of the structure's dynamic behavior) on an entire mechatronic system have to be considered by the structural optimization loop. In order to satisfy this requirement, the entire mechatronic system can be modeled as an EMBS, containing the investigated structure as an elastic body. The integration of the elastic body into an EMBS is not a trivial operation and is briefly to be abstracted now. The linear, displacement-based FE method (FEM) approximates the structures' linear elastic deformation at a certain point $\boldsymbol{u} \in \mathbb{R}^3$ by a superposition of nodal displacements $\boldsymbol{q} \in \mathbb{R}^N$ and so-called global shape functions $\boldsymbol{\Phi}$ by $\boldsymbol{u}(\boldsymbol{R}, t) = \boldsymbol{\Phi}(\boldsymbol{R}) \cdot \boldsymbol{q}(t)$, with $\boldsymbol{R}$ representing the position vector of an arbitrary material point. Since the dimension N, which is equal to the number of degrees of freedom (DOFs) of the FE model, is often very high, the entire FE model usually cannot be handled in a non-linear EMBS simulation. Therefore, it is necessary to reduce N by projecting $\boldsymbol{q}$ on a subspace $\text{span}(\boldsymbol{V}) \in \mathbb{R}^{N \times n}$ by $\boldsymbol{q}(t) = \boldsymbol{V} \cdot \boldsymbol{q}_{red}(t)$, with $n = \dim(\boldsymbol{q}_{red}) \ll \dim(\boldsymbol{q}) = N$. This step is done by

special codes for model order reduction, see e.g. (5) or (6). These tools have to provide data, that can be used in an EMBS model, e.g. the so-called standard input data (SID), see (7). There are numerous possibilities of setting up $\boldsymbol{V}$, see e.g. (8). All of them require the system matrices of the FE model as input. The delivered SID allows an EMBS simulation wherein the so-called generalized coordinates, $\boldsymbol{q}_{red}(t)$ which describe the elastic behavior of the investigated structure, can be obtained over long time intervals. Together with further information from the code for model order reduction, the so-called stress modes $\boldsymbol{\Phi}_{\sigma,red}$, the recovery of stresses during EMBS runtime is possible by $\boldsymbol{\sigma}(\boldsymbol{R},t) \approx \boldsymbol{\Phi}_{\sigma,red}(\boldsymbol{R}) \cdot \boldsymbol{q}_{red}(t)$, see (9). No additional FE solution is necessary. The derivation of the stress modes requires also the projection matrix $\boldsymbol{V}$ and some stress information which can be delivered by the FE model.

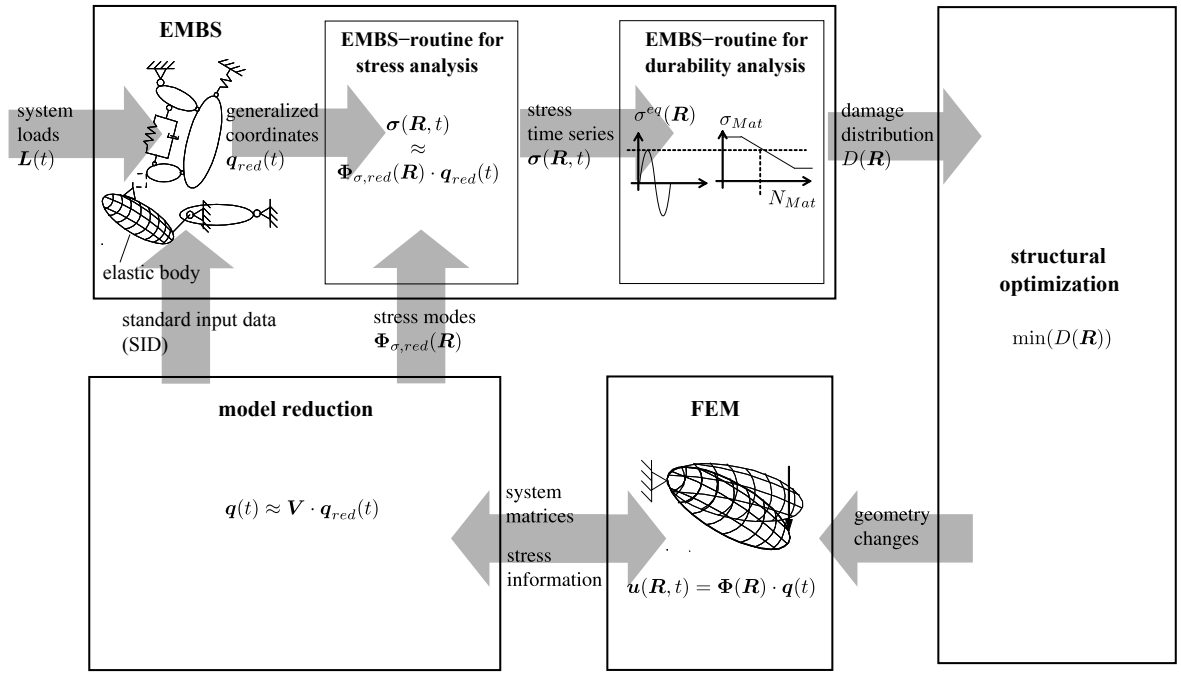

Figure 1: Optimization loop

A meaningful and appropriate method of dealing with the stress time series $\boldsymbol{\sigma}(\boldsymbol{R},t)$ is the derivation of a damage distribution $D(\boldsymbol{R})$ in the investigated structure. The resulting damage values can be used then, after appropriate definition of an utility function, as scalar performance criteria for the optimization problem. The minimization of damage $\min(D(\boldsymbol{R}))$ at the most critical locations by changes in the geometry is thus the final goal for the optimization.

3. Assorted Aspects of the Process

The proposed optimization loop of Section 2 has some special features, which are explained more precisely in the following. It works with modern model order reduction techniques based on so-called Krylov-subspaces and integrates stress respectively durability analysis in the EMBS-simulation via user-routines. The first fact is important, since model order reduction based on Krylov-subspaces delivers reduced models, which are error-free for predefined frequencies. The second fact, i.e. the 'online' stress respectively durability analysis during EMBS runtime, leads to advantageous properties of the presented loop compared to conventional approaches, like (1) or (2). A postprocessing of EMBS and FE results is not required, the tool for structural optimization can directly be interfaced with the EMBS tool.

3.1. Model Order Reduction with Krylov-Subspaces

The model order reduction technique that is used here works with so-called Krylov-subspaces. The input-output representation of the linear, undamped FE-model is

$$\begin{aligned} \boldsymbol{M}_{fem} \cdot \ddot{\boldsymbol{q}} + \boldsymbol{K}_{fem} \cdot \boldsymbol{q} &= \boldsymbol{B}_{fem} \cdot \boldsymbol{l}_{in} \\ \boldsymbol{q}_{out} &= \boldsymbol{C}_{fem} \cdot \boldsymbol{q} \end{aligned} \quad \Leftrightarrow \quad \boldsymbol{H}_{fem}(s) = \boldsymbol{C}_{fem} \cdot (s^2 \boldsymbol{M}_{fem} - \boldsymbol{K}_{fem})^{-1} \cdot \boldsymbol{B}_{fem} \qquad (1)$$

with the FE mass matrix $\boldsymbol{M}_{fem}$ and the stiffness matrix $\boldsymbol{K}_{fem}$. Matrices $\boldsymbol{B}_{fem}$ and $\boldsymbol{C}_{fem}$ are Boolean

filter matrices, which project force/torque inputs $\boldsymbol{l}_{in}$ on special interface nodes to the entire system nodes $\boldsymbol{q}$; respectively projecting the entire system nodes $\boldsymbol{q}$ to special displacement output nodes $\boldsymbol{q}_{out}$. The matrix $\boldsymbol{H}_{fem}(s)$ represents the frequency-dependent transfer function of the FE system in which $s = j\omega = j2\pi f$ (with the excitation frequency f) holds. The projection matrix $\boldsymbol{V} = \boldsymbol{V}_{kry}$ is chosen in a way that

$$\text{colsp}(\boldsymbol{V}_{kry}) \supseteq \mathcal{K}_{J_b}\left(\underbrace{\begin{bmatrix}\boldsymbol{0} & -\boldsymbol{K}_{fem}^{-1}\boldsymbol{M}_{fem}\\ \boldsymbol{I} & \boldsymbol{0}\end{bmatrix}}_{\boldsymbol{A}}, \underbrace{\begin{bmatrix}-\boldsymbol{K}_{fem}^{-1}\boldsymbol{B}_{fem}\\ \boldsymbol{0}\end{bmatrix}}_{\boldsymbol{B}}\right) \tag{2}$$

holds. This means, that the space which is spanned by the columns of the projection matrix $\boldsymbol{V}_{kry}$ comprises the space, which is spanned by the right side of Eq.(2). It holds that the (input) Krylov-subspace $\mathcal{K}_{J_b}(\boldsymbol{A}, \boldsymbol{B})$ of order J_b of the two matrices $\boldsymbol{A}$ and $\boldsymbol{B}$ is defined as $\mathcal{K}_{J_b}(\boldsymbol{A}, \boldsymbol{B}) = \text{span}[\ \boldsymbol{A},\ (\boldsymbol{A})^1\boldsymbol{B}), ...\ (\boldsymbol{A})^{J_b-1}\boldsymbol{B}\ ]$. The reduced system

$$\begin{aligned}\boldsymbol{M}_{red}\cdot\ddot{\boldsymbol{q}}_{red} + \boldsymbol{K}_{red}\cdot\boldsymbol{q}_{red} &= \boldsymbol{B}_{red}\cdot\boldsymbol{l}_{red,in}\\ \boldsymbol{q}_{red,out} &= \boldsymbol{C}_{red}\cdot\boldsymbol{q}_{red}\end{aligned} \quad \Leftrightarrow \quad \boldsymbol{H}_{red}(s) = \boldsymbol{C}_{red}\cdot(s^2\boldsymbol{M}_{red} - \boldsymbol{K}_{red})^{-1}\cdot\boldsymbol{B}_{red} \tag{3}$$

with mass matrix $\boldsymbol{M}_{red} = \boldsymbol{V}_{kry}^T\cdot\boldsymbol{M}\cdot\boldsymbol{V}_{kry}$, stiffness matrix $\boldsymbol{K}_{red} = \boldsymbol{V}_{kry}^T\cdot\boldsymbol{K}\cdot\boldsymbol{V}_{kry}$, Boolean filter matrices $\boldsymbol{B}_{red} = \boldsymbol{V}_{kry}^T\cdot\boldsymbol{B}$, $\boldsymbol{C}_{red} = \boldsymbol{C}\cdot\boldsymbol{V}_{kry}$, respectively, and transfer function matrix $\boldsymbol{H}_{red}(s)$, has advantageous properties, compare e.g. (10). Some of them are:

- The reduced model approximates the original one in the sense that the first J_b coefficients of the Taylor series expansion (the so-called moments) of the transfer functions $\boldsymbol{H}_{fem}(s)$ and $\boldsymbol{H}_{red}(s)$, compare Eq.(1) and Eq.(3), match around $s_0 = 0$.
- With little modification in the definition of the Krylov-subspace analogous to Eq.(2), the Taylor series expansion of the transfer function can be matched around arbitrary 'interesting' frequency points $s_0 \neq 0$.
- The first J_b coefficients of the Taylor series expansion of the state vector of the original model $[\boldsymbol{q},\ \dot{\boldsymbol{q}}]^T$ are equal to those of the state vector derived from the reduced model by $[\boldsymbol{V}_{kry}\cdot\boldsymbol{q}_{red},\ \boldsymbol{V}_{kry}\cdot\dot{\boldsymbol{q}}_{red}]^T$.

For a detailed description of the entire process of model order reduction with Krylov-subspace methods see e.g. (8), (10) or (11). The reduced model can be integrated in the equations of motion of an EMBS.

3.2. EMBS Simulation

The equations of motion of an ideal holonomic EMBS in the floating frame of reference formulation, see (12), with the mass matrix $\boldsymbol{M}_{mbs}$ and a vector $\boldsymbol{h}$ which collects applied, gyroscopical and elastic forces can be written as

$$\boldsymbol{M}_{mbs}(\boldsymbol{y}, \boldsymbol{q}_{red}, t)\cdot\begin{bmatrix}\ddot{\boldsymbol{y}}\\ \ddot{\boldsymbol{q}}_{red}\end{bmatrix} + \boldsymbol{h}(\boldsymbol{y}, \dot{\boldsymbol{y}}, \boldsymbol{q}_{red}, \dot{\boldsymbol{q}}_{red}, t) = \boldsymbol{0}. \tag{4}$$

Equation (4) couples the nonlinear rigid body motion of the entire mechanical system represented by $\boldsymbol{y}$ with the linear-elastic deformation of an elastic body described by $\boldsymbol{q}_{red}$. By time integration, the generalized coordinates of the EMBS $[\boldsymbol{y},\ \boldsymbol{q}_{red}]^T$ can be computed over long time intervals.

3.3. Online Stress Recovery in EMBS

By projecting the elastic coordinates $\boldsymbol{q}_{red}$ to the entire FE nodes $\boldsymbol{q} = \boldsymbol{V}_{kry}\cdot\boldsymbol{q}_{red}$, the elastic body deformation can be recovered during EMBS runtime. If a linear deformation-stress relation is assumed, also an online stress recovery is possible. The stress vector $\boldsymbol{\sigma}(\boldsymbol{R}, t)$ at a particular location $\boldsymbol{R}$ in the elastic body can be derived by

$$\boldsymbol{\sigma}(\boldsymbol{R}, t) = [\sigma_{xx},\ \sigma_{yy},\ \sigma_{zz},\ \sigma_{xy},\ \sigma_{yz},\ \sigma_{zx}]^T \approx \boldsymbol{\sigma}_{red}(\boldsymbol{R}, t) = \boldsymbol{\Phi}_{\sigma,red}(\boldsymbol{R})\cdot\boldsymbol{q}_{red}(t). \tag{5}$$

The columns of the so-called stress mode matrix $\boldsymbol{\Phi}_{\sigma,red}(\boldsymbol{R})$ are derived in a preprocessing step by loading the FE model with the associated columns of the projection matrix $\boldsymbol{V}_{kry}$, see (9).

3.4. Online Durability Analysis in EMBS

Based on the stress vector $\boldsymbol{\sigma}(\boldsymbol{R}, t)$ further calculations during EMBS runtime, like a durability analysis are possible. The online damage calculation in an EMBS can be divided into three substeps which are

- reduction of the stress vector time series to a stress intensity time series,
- reduction of the data contained in the stress intensity time series by setting up a matrix of rainflow cycles and
- comparison of this matrix of rainflow cycles with material data.

The entire process of an online durability analysis in an EMBS is described in detail in (13) or (14). In the following, only a very brief abstract is feasible. The stress vector $\boldsymbol{\sigma}(\boldsymbol{R}, t)$ can be reduced to a scalar stress intensity, e.g., like the maximum principle stress $\sigma_{pr,max}(\boldsymbol{R}, t)$ which is derived from the largest entry of the principal stress tensor. Data contained in the signal $\sigma_{pr,max}(\boldsymbol{R}, t)$ is reduced by extracting the turning points, which can be detected by a change of sign of the slope of $\sigma_{pr,max}(\boldsymbol{R}, t)$. The resulting sequence ${}^{tp}\sigma^{j}_{pr,max}(\boldsymbol{R})$, with $j = 1 \dots j_{cur}$ and j_{cur} equal to the number of turning points in the signal $\sigma_{pr,max}(\boldsymbol{R}, t)$ for the current point in time, can be scanned for closed stress cycles during EMBS runtime. Therefor a modification of the so-called '4-Point-Algorithm' is used, see (14) and references there. Closed stress cycles are important indicators for a durability analysis, since they can be set in comparison to results of Woehler-experiments, see e.g. (15). The '4-Point-Algorithm' detects closed stress cycles in a sequence of turning points and sorts them into a two dimensional matrix, wherein the maximum of a closed stress cycle is plotted over its minimum, the so-called matrix of rainflow cycles. For each of those stress cycles a damage contribution $\Delta D^{k}(\boldsymbol{R})$, with $k = 1 \dots k_{cur}$ and k_{cur} equal to the number of closed stress cycles in the sequence ${}^{tp}\sigma^{j}_{pr,max}(\boldsymbol{R})$ for the current point in time, can be calculated by a comparison with material data received from Woehler-experiments. Those damage contributions are subsequently summed up by

$$D(\boldsymbol{R}) = \sum_{k=1}^{k_{cur}} \Delta D^{k}(\boldsymbol{R}) \tag{6}$$

to receive a total damage value $D(\boldsymbol{R})$ for the current point in time.

4. Example Model

The example model, which is used is a chaotic pendulum, see the left side of Figure 2. It is released from a non-rest position and gravity points in the negative y-direction. The carrier body of the chaotic pendulum is modelled as an elastic body. Force and constraint elements can be attached to the carrier via three massless plates which coincide with the carrier's planar faces in positive x- (front), positive y- (top) and negative x-direction (back). Those plates are connected to the carrier's corner nodes via multipoint constraints. The top massless plate is coupled at its center with a revolute joint around the z-axis to the inertial system (Isys). Two rigid pendulum rods are attached to the carrier at the centers of the front and back massless plate, respectively with revolute joints also around the z-axis.

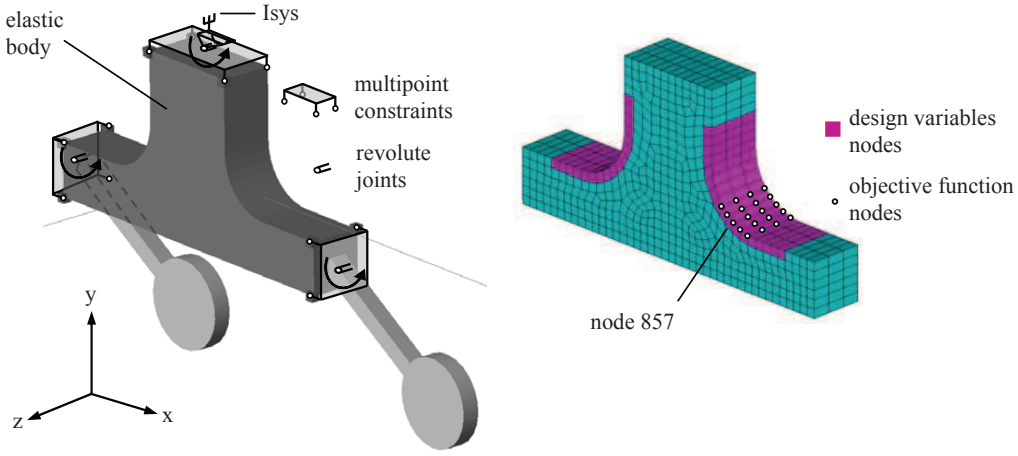

Figure 2: Example model

The FE model which is associated to the elastic carrier has 5700 displacement DOFs. Its dimension is reduced with model order reduction based on Krylov-subspaces, see Section 3.1. As interesting reduction

frequency 2 Hz is chosen, since the eigenfrequencies of the linearized EMBS model are in this range, compare Table 2. Input- and output-DOFs in the sense of Eqs. (1) and (3) are the $3 \cdot 6$ DOFs which describe the rigid body motion of the front, top and back massless plate, wherewith the carrier is coupled to other components of the EMBS. The model order reduction with Krylov-subspaces results in 18 generalized coordinates that describe the elastic behavior of the carrier.
The dynamic behavior of the chaotic pendulum, which is simulated here for 2 s, causes dynamic stresses inside the carrier body, which on their part lead to a damage distribution. The optimization problem is formulated in such a way, that the maximum damage in the area of the objective function nodes, compare the right side of Figure 2, has to be minimized. Therefor, the optimization algorithm is allowed to move the so-called design variables nodes, which are also illustrated in Figure 2. Also, three optimization constraints are introduced. The total mass of the carrier body has to remain constant, the carrier body's symmetry with respect to the yz-plane has to be kept during the optimization and changes in its cross-sections orthogonal along the z-direction are not allowed, i.e. the carrier has to be stampable. As a special node where some results are exemplarily postprocessed, the node with number 857 is chosen. To keep results surveyable, the maximum number of optimization iterations is restriced to ten.

5. Results

The results that are presented here comprise results referring to the quality of the reduced FE model (Sections 5.1 til 5.3) and referring to the properties of the entire EMBS model (Sections 5.4 til 5.6). The state before the optimization is also called 'iteration: 0' in the following, the state after the optimization is also called 'iteration: 10'.

5.1 Eigenfrequencies of the FE-models

The lowest six eigenfrequencies of the entire free FE model, see Eq. (1), before the optimization and those of the reduced free FE model, see Eq. (3), before and after the optimization are listed in Table 1.

Table 1: Eigenfrequencies of the free FE models before and after the optimization

eigenfrequency [no.]	entire [Hz] (reference) iteration: 0	reduced [Hz] iteration: 0	reduced [Hz] iteration: 10
1	41.6060	46.0735	47.1889
2	51.0600	56.6336	60.2383
3	68.5056	58.9306	64.8665
4	71.3864	89.7623	93.4568
5	93.5641	126.8091	131.0851
6	93.5673	128.9013	132.6043
...	...	...	...

The eigenfrequencies of the reduced model do not match the eigenfrequencies of the entire FE model for the initial iteration. This is not very surprising, since the model order reduction based on Krylov-subspaces is done for a frequency of 2 Hz, see Section 4, and the lowest eigenfrequency of approximatly 41 Hz is far apart from this 'interesting' frequency. A comparison of the initial and last iteration shows, that the optimization itself does not dramatically influence the carrier's eigenfrequencies. It can be recorded, that the optimization algorithm stiffens the carrier.

5.2 Relative Error in the Transfer Function

More detailed information about the quality of the reduced model can be obtained, when looking at the relative error between the transfer functions of the entire and reduced models. The Frobenius norm of this relative error $\epsilon_H(s)$ is calculated by

$$\epsilon_H(s) = \frac{||\boldsymbol{H}_{fem}(s) - \boldsymbol{H}_{red}(s)||_F}{||\boldsymbol{H}_{fem}(s)||_F} \tag{7}$$

with $\boldsymbol{H}_{fem}$ from Eq. (1) and $\boldsymbol{H}_{red}$ from Eq. (3). This relative error norm is plotted in Figure 3 for a frequency range from 0 to 100 Hz.

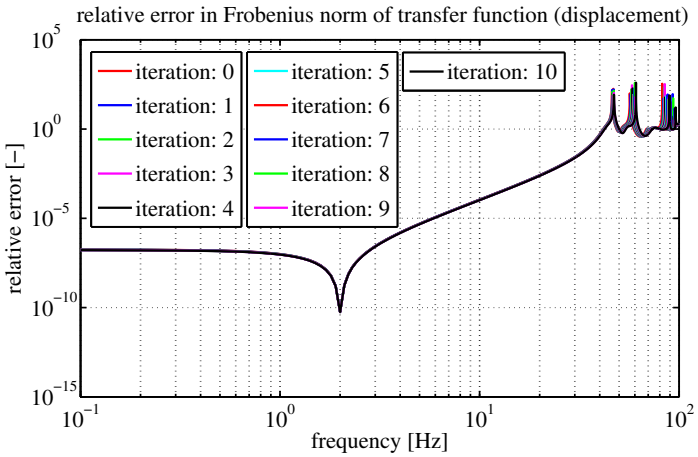

Figure 3: Relative error in the transfer function during the optimization

Results confirm the error-free input-output behavior of the reduced model for the 'interesting' frequency of 2 Hz. The error norm shows a 'dropping' for this frequency. Furthermore, Figure 3 delivers information about the usability of the reduced model. If a relative error of 10^{-3} is tolerable, the reduced model delivers acceptable results up to 20 Hz.

5.3 Relative Error in the Stress Tensor

Also the relative error in the stress tensor can be investigated. This is done here by a exemplaric load case. The free carrier is loaded at the center of the top plate with an harmonic force of amplitude 1 N in y-direction. The frequency-dependent stress amplitudes of the stress tensor in node 857 are accordingly recorded.

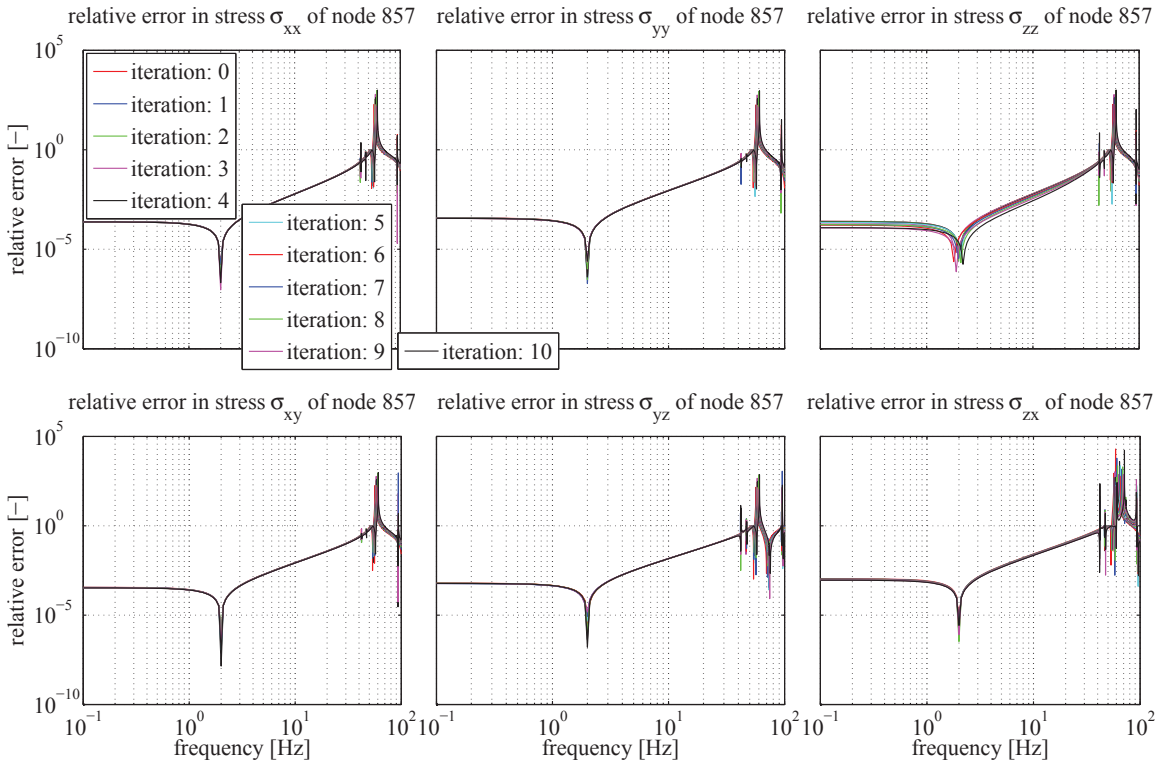

Figure 4: Relative error in stress tensor of node 857 during the optimization

The relative errors $\epsilon_{\sigma,ij}(s)$ which result from

$$\epsilon_{\sigma,ij}(s) = \frac{|\sigma_{ij,fem}(s) - \sigma_{ij,red}(s)|}{|\sigma_{ij,fem}(s)|} \quad \text{with} \quad i,j \in [x,y,z] \tag{8}$$

and $\sigma_{ij,fem}$ representing the stress tensor entry according to the FE solution and $\sigma_{ij,red}$, the associated entry from the reduced model, are plotted for node 857 in Figure 4. The reduced model delivers correct stress values for the reduction frequency of 2 Hz for all iterations. The model order reduction with Krylov-subspaces allows an automated error-free stress recovery for predefined frequencies, independent from the current FE mesh, which is controlled by the optimization. Since single precision is used for the stress-error computation all values below 10^{-6} are considered as zero.

5.4 Eigenfrequencies of the EMBS-models

After investigating the separated FE model of the carrier, the entire EMBS model is analyzed. Firstly the system is linearized at its rest position and the resulting lowest three eigenfrequencies are listed in Table 2.

Table 2: Eigenfrequencies of the EMBS models before and after the optimization

eigenfrequency [no.]	rigid [Hz] (reference) iteration: 0	elastic [Hz] iteration: 0	elastic [Hz] iteration: 10
1	1.2318	1.2251	1.2261
2	2.2204	2.2189	2.2190
3	2.6212	2.6095	2.6101
...	-	...	...

Table 2 comprises the eigenfrequencies of the EMBS models before and after the optimization. Also here, the stiffening caused by the optimization algorithm can be observed. As reference, the results of the rigid MBS-model, which belongs to the initial iteration, is listed.

5.5 Stress Time Series

Furthermore, the stress time series for the entire EMBS load case are interesting. Hereby the time series of the maximum principle stress in node 857 is investigated and plotted in Figure 5.

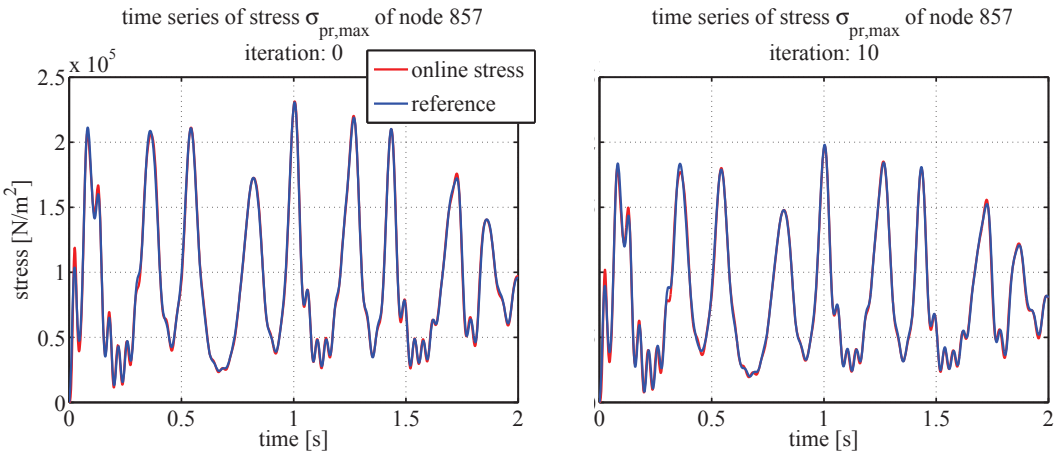

Figure 5: Time series of maximum principle stress of node 857 before and after the optimization, comparison with reference solution

The figure also includes a kind of reference solution, which is calculated by a method proposed in (16). It can be stated, that the stress time series, which is calculated online, compare Section 3.3, matches the reference solution very well. Nevertheless, there are slight differences between the two graphs. This difference can be explained by two facts. Firstly, the reference according to (16) is also an approximation

of an entire transient FE solution and therefore defective. Secondly, both solutions differ in the SID which is used for the EMBS simulation, compare Figure 1 and Section 2. Therefore, the equations of motion, see Eq.(4), have slightly different solutions, a fact that also effects the calculated dynamic stresses. In addition to the good approximation of the reference solution, the effects of the optimization algorithm work can be seen in Figure 5. In total, the maximum principle stress in node 857 is reduced by the geometry changes of the optimization algorithm.

5.6 Matrices of Rainflow Cycles and Damage

After the derivation of the stress time series, durability calculations can be carried out. Figure 6 shows the matrix of rainflow cycles of the maximum principle stress in node 857 during the optimization.

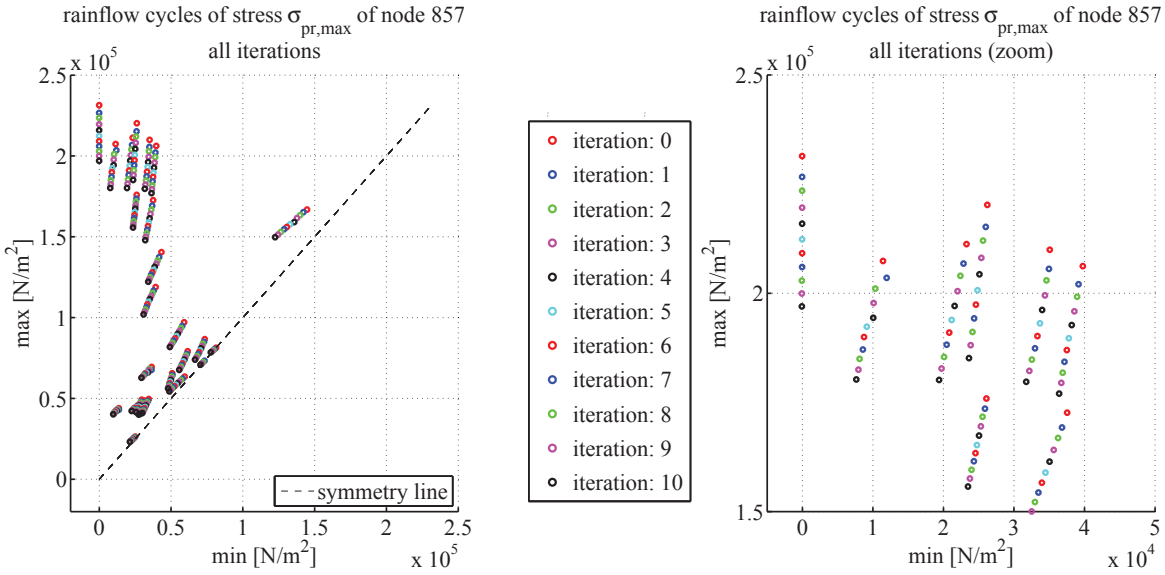

Figure 6: Rainflow matrix for maximum principle stress of node 857 during the optimization

The figure nicely overviews the optimization progress. It should be kept in mind, that a movement of the points in the matrix in the direction of the zero-point $(0, 0)$ represent lower stress amplitudes and, therefore, lower damage values. The zoom view at the right side of Figure 6 clarifies this movement. The equidistant step size between the different iterations suggests, that the optimization has not yet converged after ten iterations and further improvement is possible by not constricting the maximum number of iterations.

Table 3: Damage values and repeatability for node 857 before and after the optimization

node [no.]	log(damage) iteration: 0	log(damage) iteration: 10	repeatability iteration: 0	repeatability iteration: 10	factor
857	-15.9437	-16.2846	8.7842E+15	1.9258E+16	2.19

Table 3 summarizes the results of the online damage calculation and lists the logarithm of the damage value, compare Eq. (6), in node 857 before and after the optimization. Since this value is not very handy, a repeatability value $N(\boldsymbol{R}) = 1/D(\boldsymbol{R})$ is derived from the damage value $D(\boldsymbol{R})$. The repeatability holds the information how many times the chosen load case can be applied to the structure until failure occurs. In this example, the repeatability can be more than doubled.

5.7 Shape

Concluding the optimization results, the shape of the carrier is visualized in the following. Figure 7 shows a cross-section of the carrier's radius where the considered nodes are located. On the left side the initial design is presented, the middle subfigure shows the last design after ten iterations and on the right side

both designs can be compared by a superimposing. Here the redistribution of material which is necessary to fullfill the constraint of constant mass, can be observed. The plots are colored with the logarithms of the resulting damage values, but the given color scale is only valid for the design variables nodes on the surface, compare Figure 2. For the internal nodes and nodes close to the multipoint constraints, no damage is calculated. (Those nodes are colored in gray in Figure 7 and Figure 8.)

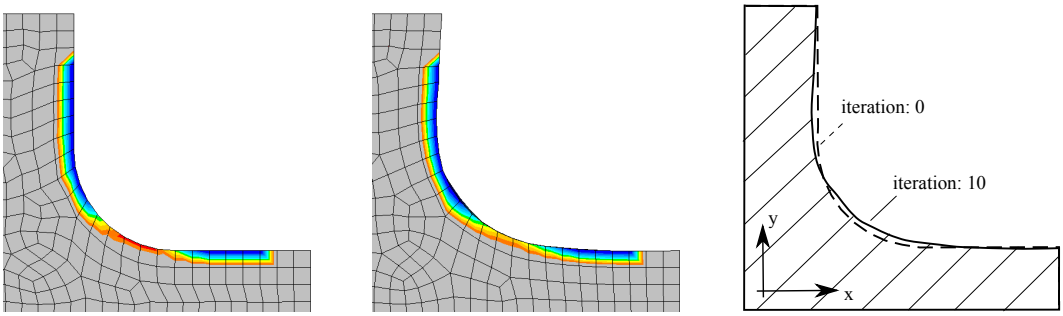

Figure 7: Shape optimization, cross-section of the optimized area

The view of the carrier in Figure 8 illustrates the results of Table 3. Damage values in the design area are considerably reduced from the initial design on the left side to the final design on the right side. Furthermore it can be observed, that the symmetry and stampability constraints are fullfilled.

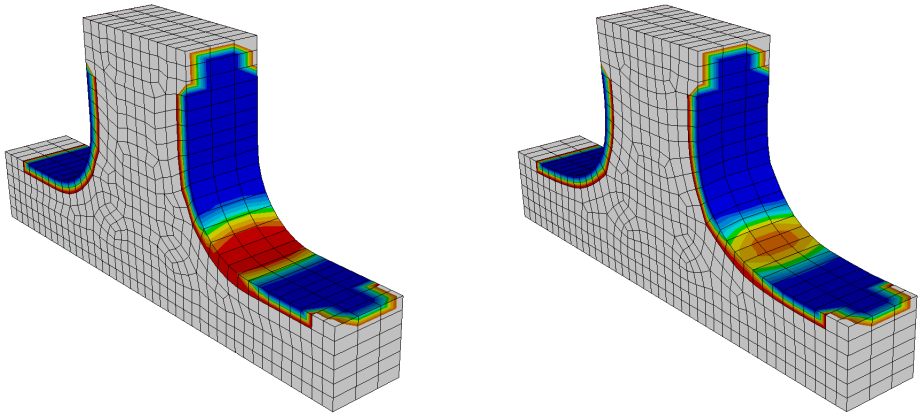

Figure 8: Shape optimization, perspective view

6. Conclusions

The contribution proposes a loop for structural optimization in which the effects of the structural optimization on an EMBS are considered. Damage values that are calculated during EMBS runtime serve as scalar performance criteria for the structural optimization. Thereby the EMBS can directly be interfaced with the optimization algorithm and no postprocessing of EMBS and FE results is necessary. The contribution shows with the help of an example model, that for any intermediate result of the optimization an error-free recovery of stresses for predefined frequencies is possible. Therefore, also error-free damage values can be expected. These findings encourage further studies. By improving the optimization loop a 'controlled' model order reduction might be integrated. This would allow error-free EMBS results for predefined frequency ranges. This is a circumstance that seems to be beneficial if structural optimization is done with extreme geometry changes, like e.g. in a topology optimization.

Acknowledgements

The authors would like to thank the company FE-Design GmbH for the provision of the software Tosca (3) and the company Simpack AG for providing the software Simpack (17) for this project. Also the associated kind support regarding both software tools is gratefully acknowledged.

References

[1] Häußler, P.: Ein neuer Prozess zur parameterfreien Formoptimierung dynamisch beanspruchter Bauteile in mechanischen Systemen auf Basis von Lebensdaueranalysen und hybriden Mehrkörpersystemen, (in German), Vol. 20. Universität Karlsruhe: Forschungsberichte aus dem Institut für Produktentwicklung und Konstruktion, 2005.

[2] Tobias, C.; Eberhard, P.: Durability-based Topology Optimization of a Steering System. In Proceedings of the 8th World Congress on Structural and Multidisciplinary Optimization, Lisbon Portugal, 2009.

[3] FE-Design: Tosca Structure, General Documentation, Tosca Version 6.1. FE-Design GmbH, Karlsruhe, 2007.

[4] Harzheim, L.: Strukturoptimierung, Grundlagen und Anwendungen (in German). Frankfurt: Verlag Harri Deutsch, 2008.

[5] Simpack: FEMBS, Reference Guide, Simpack Version 8.901b. Simpack AG, Gilching, 2009.

[6] Fehr, J.; Eberhard, P.: Simulation Process of Flexible Multibody Systems with Advanced Model Order Reduction Techniques (submitted for publication). Multibody System Dynamics, 2010.

[7] Wallrapp, O.: Standardization of Flexible Body Modeling in Multibody System Codes, Part I: Definition of Standard Input Data. Mechanics of Structures and Machines, Vol. 22, No. 3, pp. 283–304, 1994.

[8] Lehner, M.: Modellreduktion in elastischen Mehrkörpersystemen (in German). Dissertation, Schriften aus dem Institut für Technische und Numerische Mechanik der Universität Stuttgart, Band 10. Aachen: Shaker Verlag, 2007.

[9] Tobias, C.; Eberhard, P.: Stress Recovery with Krylov-Subspaces in Reduced Elastic Multibody Systems (submitted for publication). Multibody System Dynamics, 2010.

[10] Salimbahrami, S.B.: Structure Preserving Order Reduction of Large Scale Second Order Models. Ph.D. thesis, Technische Universität München, 2005.

[11] Bai, Z.: Krylov Subspace Techniques for Reduced-order Modeling of Large-scale Dynamical Systems. Applied Numerical Mathematics, Vol. 43, pp. 9–44, 2002.

[12] Schwertassek, R.; Wallrapp, O.: Dynamik flexibler Mehrkörpersysteme (in German). Braunschweig: Vieweg, 1999.

[13] Humke, T.: Implementierung einer Routine zur Schädigungsberechnung in einem elastischen Mehrkörpersystemen (in German). Studienarbeit, Institute of Engineering and Computational Mechanics, University of Stuttgart, 2010.

[14] Tobias, C.; Eberhard, P.: Berechnung von Schädigungswerten zur EMKS-Laufzeit (in German). Institutsinterne Aufzeichnung ITMCT100002, Institute of Engineering and Computational Mechanics, University of Stuttgart, 2010.

[15] Bannantine, J.A.; Corner, J.J.; Handrock, J.L.: Fundamentals of Metal Fatigue Analysis. Upper Saddle River: Prentice Hall, 1990.

[16] Eichberger, A.; Dietz, S.: Fatigue Analysis on a Virtual Test Rig Based on Multi-Body Simulation. In: Multi-body Dynamics - Monitoring and Simulation Techniques - III, Rahnejat H. and Rothberg S. (Eds.). New York: John Wiley & Sons, 2004.

[17] Simpack: Simpack, Reference Guide, Simpack Version 8.901b. Simpack AG, Gilching, 2009.